REDUCTION OF POTENTIAL RADIOLOGICAL RISKS FOR PATIENTS UNDERGOING DIAGNOSTIC EXAMS THROUGH MODIFICATION OF THE X-RAY SPECTRUM

REDUCCIÓN DE RIESGOS RADIOLÓGICOS POTENCIALES PARA PACIENTES SOMETIDOS A EXÁMENES DE DIAGNÓSTICO MEDIANTE LA MODIFICACIÓN DEL ESPECTRO DE RAYOS X

José Santa Cruz Delgado[1], Fernando Márquez Pachas[2,3], Alberto E. Gonzales-Ccoscco[4,5*], Eduardo Carrasco Solís[3,6] Carlos Herrera Castillo[3], Galo Patiño Camargo[6] and Mirko Alva-Sánchez[7]

[1] Universidad Peruana Cayetano Heredia, Unidad de Formación Básica e Integral, Lima, Perú.
[2] Universidad Peruana Cayetano Heredia, Facultad de Medicina, Lima, Perú.
[3] Instituto Nacional de Enfermedades Neoplásicas, Surquillo, Departamento de Radioterapia, Lima, Perú.
[4] Universidad Tecnológica del Perú, Lima, Perú.
[5] Universidade Federal de Uberlândia, Programa de Pós-Graduação em Engenharia Biomédica, Uberlândia, Brasil.
[6] Universidad Nacional de San Marcos, Lima Cercado, Facultad de Ciencias Físicas, Lima, Perú.
[7] Universidade Federal de Ciências da Saúde de Porto Alegre, Rua Sarmento Leite 245, Grupo de Física Médica Experimental e Computacional, Porto Alegre, CEP 90050-170, Brasil.

(Received: feb./2024. Accepted: may./2024)

Abstract

The diagnostic medical practice using X-rays significantly contributes to the collective dose worldwide, where the inherent risk in each examination is proportional to the absorbed dose, which is related to deterministic and stochastic effects of ionizing radiation. Therefore, due to the necessity of optimizing each radiological procedure, this study aimed to reduce the absorbed dose in patients undergoing X-ray examinations by evaluating each parameter that modifies the spectral distribution. The Birch and Marshall method was employed to reconstruct and modify the X-ray spectra based on tube voltage, filtration, tube current, anode angle, and energy pass factor.

* betoagc@hotmail.com doi: https://doi.org./10.15446/mo.n69.115340

By modifying these parameters, it was possible to reduce the absorbed dose in the patient's skin by up to 38%. The proposed methodology is feasible for implementation in clinical centers, given the availability of copper filters incorporated into X-ray equipment. Additionally, an alternative technique involving tantalum filters is presented, achieving a reduction in absorbed dose of up to 57%. Thus, with the developed methodology, it is demonstrated that it is possible to reduce radiation doses by modifying spectral distributions, reproducing medical images with a significant reduction in the absorbed dose on the patient, while ensuring quality and safety in X-ray diagnostic procedures.

Keywords: X-ray spectrum, absorbed dose, filtration, copper filters, radiographic technique.

Resumen

La práctica médica diagnóstica con rayos X contribuye ampliamente a la dosis colectiva a nivel mundial, donde el riesgo inherente en cada examen es proporcional a la dosis absorbida, que está relacionado con los efectos determinísticos y estocásticos de la radiación ionizante. Así, debido a la necesidad de optimizar cada procedimiento radiológico, este trabajo tuvo el objetivo de reducir la dosis absorbida en pacientes sometidos a los exámenes con rayos X mediante la evaluación de cada uno de los parámetros que modifican la distribución espectral. Se utilizó el método de Birch y Marshall para reconstruir y modificar los espectros de rayos X en función del voltaje de tubo, la filtración, la corriente de tubo, el ángulo del ánodo y el factor de paso para la energía. Modificando estos parámetros se logró reducir la dosis absorbida en la piel del paciente hasta un 38%. La metodología propuesta es factible para la implementación en centros clínicos, debido a la disposición de filtros de cobre, los cuales están incorporados en los equipos de rayos X. Así como también, en forma alternativa, se muestra la técnica con inserción de filtros de tantalio con el cual se reduce la dosis absorbida hasta un 57%. Así, con la metodología desarrollada, se demuestra que es posible

reducir las dosis de radiación, modificando las distribuciones espectrales, las cuales reproducen las imágenes médicas con una reducción significativa de la dosis absorbida sobre el paciente, garantizando al mismo tiempo la calidad y seguridad en los procedimientos de diagnóstico con rayos X.

Palabras clave: espectro de rayos X, dosis absorbida, filtración, filtros de cobre, técnica radiográfica.

Introduction

Currently, digital radiology has the significant potential to enhance the quality of medical imaging, providing greater opportunities for accurate and timely diagnosis. However, this technique comes with an increased radiation dose compared to conventional radiology, leading to an elevated radiological risk. The landscape of digital radiology underscores the need to reinforce justification and optimization processes, particularly in minimizing the dose at the skin's entrance surface for each radiological procedure [1].

On the other hand, there is currently experiencing an exponential increase in the use of radiological techniques for diagnostic purposes. In many cases, this practice is not adequately justified, and there is also excessive use of exposures in interventional radiology. All of this, combined with a lack of knowledge about radiation doses in these practices, is of particular concern to dedicated physicians and physicists. The reduction of dose at the skin's surface is crucial in mitigating the risk of side effects such as erythema and burns. Additionally, it helps avoid the risk of diagnostic errors due to a decrease in image quality. To date, a variety of accidents in diagnostic and interventional X-ray practices have been reported [2]. In Peru, at a level III healthcare institution, a radio induced dermal injury occurred in a patient during the application of a fluoroscopy-guided radiological procedure [3, 4].

Let's also consider that risks associated with radiation-induced effects on a patient's skin can vary significantly depending on the

type of X-ray examination [5, 6], the anatomical area examined, the patient's age, gender, and other individual factors. This emphasizes the importance of assessing skin doses for different types of examinations.

There are studies that have demonstrated the effectiveness of reducing skin dose using metallic filters that modify the X-ray spectrum [5]. However, it is essential to consider that these filters also alter image quality and the absorbed doses in various exposed organs (due to the modification of the effective energy of the beam). Additionally, implementing the strategy of modifying the X-ray spectrum with metallic filters in clinical practice poses a challenge because it necessitates adjustments to the clinical beam, specialized accessories, and the lack of training among professionals in these strategies.

Monte Carlo simulations are a powerful tool for calculating the deposited dose on the skin surface or other surrounding regions. Currently, there are various packages for such simulations, and in this study, the PENELOPE package version 2018 [7] was utilized. This package simulates the coupled transport of electrons and photons in arbitrary materials over a broad energy range, from a few hundred eV to approximately 1 GeV.

The objective of this research is to reduce the absorbed dose received by patients undergoing chest X-ray examinations while maintaining image quality. This is achieved through the evaluation of each parameter that modifies the spectral distribution using two software tools, XSPMAS and XCOMP5R, which generate X-ray energy spectra. The PENELOPE code was also employed to simulate different clinical examination scenarios with various filters [6, 8, 9].

In this sense, we proceeded to compare the results of different proposed radiographic techniques denoted as T1 to T7, with a reference technique (T0).

Materials and Methods

The methodology outlined for generating the X-ray spectrum has been implemented through computational simulation using the XSPMAS algorithm [8]. Additionally, X-ray spectra were computed employing the Monte Carlo technique with the XCOMP5R program [9], along with an analysis of the electron interaction process with the tungsten target. For all programs, input parameters include the applied voltage to the X-ray tube, anode angle, mAs, as well as the material and thickness of the filter. The resulting variables are the spectrum intensity (differential X-ray fluence rate) and the mean energy. The X-ray spectra computed by the XCOMP5R program are utilized in the "*input.in*" file of the PENELOPE code to simulate the clinical beams employed in each radiological technique.

Reproduction of the X-ray Spectrum

It was computed employing the theory established by Birch and Marshall [8, 10], in which the intensity of the continuous X-ray spectrum for a solid target, generated by an electron traversing a distance dx in an element, is provided by:

$$dI(E) = Q\frac{N_a}{A}\rho\, dx \tag{1}$$

where N_a is Avogadro's number, A is the atomic weight of the target, ρ is its density, and Q is the energy intensity per unit energy interval per incident electron per atom per mm^2 of area at 0.75 m. Thus, by integrating equation (1), the energy intensity is obtained [8, 10]:

$$I(E) = \frac{\rho N_a}{A}\int_{T_0}^{E} Q\left(\frac{dT}{dx}\right)^{-1} dT \tag{2}$$

where the stopping power dT/dx is the continuous loss of kinetic energy (T) by the electron as it interacts with the atoms of the

target. This loss is given by Whiddington [8, 10]

$$T = (T_0^2 - \rho C x)^{\frac{1}{2}} \tag{3}$$

where C is the Thomson-Widdington constant, which for energies above 60 keV depends on the initial energy as follows [8, 10]:

$$C = (0.0029 T_0 + 0.41) \times 10^6 \left(\frac{\text{keV}^2\,\text{cm}^2}{g} \right) \tag{4}$$

$$y = \frac{T_0^2 - T^2}{\rho C} \cot\theta \tag{5}$$

Taking into account the anode effect, represented by $e^{-\mu_w(E)y}$, where $\mu_w(E)$ is the attenuation coefficient of tungsten for energy E. Ultimately, the energy intensity can be formulated as [8, 10]:

$$I(E) = \frac{\rho N_a}{A} \int_{T_0}^{E} \left(1 + \frac{T}{m_0 c^2} \right) e^{\left[-\left(\frac{\mu_w(E)}{\rho C} (T_0^2 - T^2) \cot\theta \right) \right]} Q \left(\frac{dT}{dx} \right)^{-1} dT \tag{6}$$

Equation (6) provides the energy intensity of an X-ray spectrum for each energy E in units of J/mAs mm^2 keV at a distance of 75 cm from the X-ray source [8, 10]. On the other hand, the intensity of the characteristic X-ray spectrum is proportional to the difference between the energy of the incident electron and the binding energy of the K-shell raised to the power of 1.63, as described by [11, 12]:

$$I_K = \text{const}(T_0 - E_K)^{1.63} \tag{7}$$

where E_K is the binding energy of the K-shell, and T_0 is the kinetic energy of the incident electrons.

The KERMA (Gy) was determined by considering its dependence on the energy fluence distribution at energy Ψ_E(as well as on the energy fluence distribution at energy Φ_E), as described in [13, 14]

$$K = \int_E \Psi_E \frac{\mu_{tr}(E)}{\rho} dE = \int_E E \Phi_E \frac{\mu_{tr}(E)}{\rho} dE \tag{8}$$

where $\dfrac{\mu_{tr}(E)}{\rho}$ is the mass energy transfer coefficient of those uncharged particles in the specified material.

The equations developed by Birch and Marshall (1979) were implemented by Córte Brochi (1990) in the XSPMAS software [8, 10], and the results for the X-ray spectrum obtained were compared with those generated by the XCOMP5R program (based on the Monte Carlo technique) [9].

Optimization of Radiological Techniques

Reference radiographic technique: It was employed a standard chest imaging protocol as the reference technique for a patient weighing between 60 kg and 70 kg, following the procedures used at the National Institute of Neoplastic Diseases (INEN- in spanish *Instituto Nacional de Enfermedades Neoplásicas*): 125 kVp, filter (2.8 mmAl + 0.1 mmCu), 2 mAs, and a source-to-surface distance (SSD) of 150 cm.

Definition of proposed radiological techniques: A total of 418 radiological techniques (kV, Filtration, mAs, SSD) were defined, with an interval of ± 10 kV from the reference technique, at 2 kV intervals. These techniques were reproduced using the XSPMAS and XCOMP5R programs, resulting in the average energy (keV) and photon fluence (photons/mm^2 at a focus-to-distance of 0.75 m)

As the reference technique (chest) is conducted at a 150 cm Source-to-Skin Distance (SSD), while the software reports fluence calculations at 75 cm, normalization of fluence values is necessary (using the inverse square law) to align them with an SSD of 75 cm for comparative analysis of fluence spectra and radiation doses. For the assessment of depth dose percentages, normalization is applied to an SSD of 100 cm. This approach is justified by the assumption that the percentage reduction in radiation dose remains consistent across different SSDs.

Optimization with Respect to the Reference Mean Energy of 62.3 keV: Considering a range of +2 keV, we selected 101 techniques, including the reference technique, within the range of

(62.3 – 64.3) keV. The +2 keV interval in the mean beam energy is applied to uphold and enhance image quality. Figure 1 and Table 1 illustrate the dependency of Mean Energy on added filtration, while Figure 2 and Table 2 present fluence values based on the thickness of the added filter for each radiological technique.

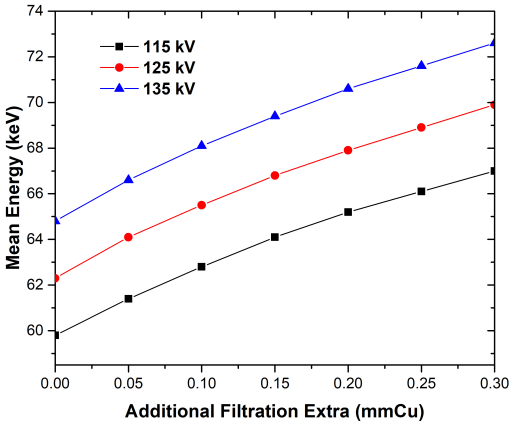

FIGURE 1. *Mean energy as a function of added filter thickness*

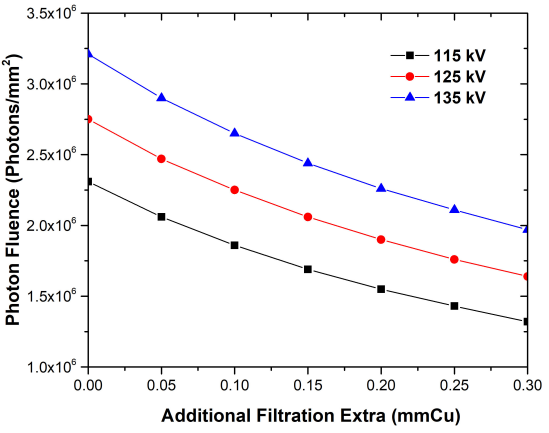

FIGURE 2. *Photon fluence as a function of added filter thickness*

MEAN ENERGY (keV)							
Inherent filtration: (2.8 mmAl + 0.1 mmCu; anode angle = 12°)							
	Extra additional filtration (mmCu)						
kV	**0.00**	**0.05**	**0.10**	**0.15**	**0.20**	**0.25**	**0.30**
115	59.8	61.4	62.8	64.1	65.2	66.1	67.0
117	60.3	62.0	63.4	64.6	65.7	66.7	67.6
119	60.8	62.5	63.9	65.2	66.3	67.3	68.2
121	61.3	63.0	64.5	65.7	66.8	67.8	68.8
123	61.8	63.5	65.0	66.2	67.4	68.4	69.3
125	**62.3**	64.1	65.5	66.8	67.9	68.9	69.9
127	62.9	64.6	66.0	67.3	68.5	69.5	70.5
129	63.4	65.1	66.5	67.8	69.0	70.0	71.0
131	63.9	65.6	67.0	68.3	69.5	70.6	71.6
133	64.3	66.1	67.6	68.9	70.0	71.1	72.1
135	64.8	66.6	68.1	69.4	70.6	71.6	72.6

TABLE 1. *Mean energy values by proposed radiological technique*

PHOTON FLUENCY (photon/mm^2)							
Inherent filtration: (2.8 mmAl + 0.1 mmCu; anode angle = 12°)							
	Extra additional filtration (mmCu)						
kV	**0.00**	**0.05**	**0.10**	**0.15**	**0.20**	**0.25**	**0.30**
115	2.3E+06	2.0E+06	1.9E+06	1.7E+06	1.6E+06	1.4E+06	1.3E+06
117	2.4E+06	2.1E+06	1.9E+06	1.8E+06	1.6E+06	1.5E+06	1.4E+06
119	2.4E+06	2.2E+06	2.0E+06	1.8E+06	1.7E+06	1.6E+06	1.5E+06
121	2.5E+06	2.3E+06	2.1E+06	1.9E+06	1.8E+06	1.6E+06	1.5E+06
123	2.7E+06	2.4E+06	2.2E+06	2.0E+06	1.8E+06	1.7E+06	1.6E+06
125	**2.8E+06**	2.6E+06	2.3E+06	2.1E+06	1.9E+06	1.8E+06	1.6E+06
127	2.8E+06	2.6E+06	2.3E+06	2.1E+06	2.0E+06	1.8E+06	1.7E+06
129	2.9E+06	2.7E+06	2.4E+06	2.2E+06	2.0E+06	1.9E+06	1.7E+06
131	3.0E+06	2.7E+06	2.5E+06	2.3E+06	2.1E+06	2.0E+06	1.8E+06
133	3.1E+06	2.8E+06	2.6E+06	2.4E+06	2.2E+06	2.0E+06	1.9E+06
135	3.2E+06	2.9E+06	2.7E+06	2.4E+06	2.3E+06	2.1E+06	2.0E+06

TABLE 2. *Photon fluence values by proposed radiological technique*

Optimization at the second level (based on photon fluence): The reference photon fluence stands at 1.1E+07 photons/mm^2 at a distance of 75 cm. Acknowledging the direct proportionality of absorbed dose to fluence, we identified the minima of the fluence function (refer to Figure 3), incorporating the criterion of fluence reduction in comparison to the reference technique (T0). Consequently, seven (07) techniques were selected from the pool of 101 techniques that successfully passed the first level. These chosen techniques are detailed in Table 3. Notably, Technique T1, featuring tantalum filtration, demonstrates the most significant reduction in fluence, while T2 achieves a higher percentage reduction in fluence using copper filters.

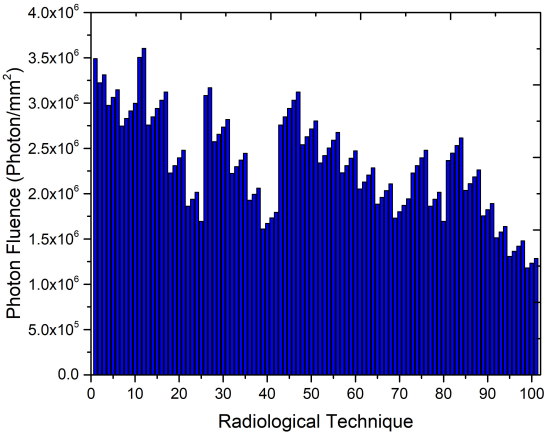

FIGURE 3. *Photon fluence as a function of the proposed radiological technique, for an average energy between 62.3 - 64.3 keV*

Monte Carlo Simulations

Computational simulations were conducted using the Monte Carlo package PENELOPE, version 2018. A cubic water phantom with dimensions of 40 × 40 × 20 cm^3 was modeled to represent the dimensions of a patient undergoing chest examinations. A radiation field of 10 × 10 cm^2 was projected at a source-to-surface distance of 100 cm. The parameters used in the simulation were: KPAR - type of primary particle (electron, photon, or positron); $\mathbf{E_{ABS}}$ - simulation cutoff energy representing the highest value

Radiological Technique	kV	Total Filtration				Mean Photon Energy (keV)	Photon Flux at 0.75 m (Photons/mm^2)	Reduction of Fluence (%)
		Inherent (mmAl)	Additional Fixed (mmCu)	Additional Extra				
T0(*)	**125**	**2.8**	**0.10**	**Has not**		**62.3**	**1.1E+07**	**0.00**
T1	115	2.8	0.10	60	μmTa	62.9	4.7E+06	**57.2**
T2	115	2.8	0.10	0.15	mmCu	64.1	6.7E+06	**38.6**
T3	115	2.8	0.10	3.0	mmAl	62.3	6.9E+06	**37.3**
T4	117	2.8	0.10	3.0	mmAl	62.9	7.2E+06	**34.7**
T5	115	2.8	Has not	0.20	mmCu	62.8	7.4E+06	**32.5**
T6	119	2.8	0.10	3.0	mmAl	63.4	7.5E+06	**32.1**
T7	117	2.8	0.10	2.5	mmAl	62.5	7.5E+06	**31.7**

TABLE 3. *Proposed radiological techniques (2 mAs, 75 cm SSD) whose photon fluence shows an acceptable percentage reduction, where T0 is the reference technique*

the particle possesses before being locally absorbed; C1 - defines the average angular deflection produced by multiple scatterings occurring between consecutive hard elastic events; this value can vary between 0 and 0.2; C2 - defines the maximum fraction of energy lost (on average) between consecutive hard elastic events; this value can vary between 0 and 0.2;W_{CC} - cutoff energy (eV) for inelastic collisions; W_{CR} - cutoff energy for hard bremsstrahlung emissions (eV). For all simulations, these parameters have been configured with specific values: EABS (1:3) = 5×10^3 eV, C1 = 0.05, C2 = 0.05, $W_{CC} = 2 \times 10^3$, and $W_{CR} = 2 \times 10^3$. The dose distribution, analyzed concerning depth, was computed with a spatial resolution of $0.2 \times 0.2 \times 0.2$ cm^3. The Monte Carlo simulations yielded data with statistical uncertainties below 1% for a set of 2×10^9 primary histories.

Results and Discussion

To assess the quality of the technique, key variables such as mean energy, photon fluence, and air KERMA were employed. The appropriateness of image quality serves as the primary indicator. The corresponding values are detailed in Table 4 and Table 5,

highlighting maximum deviations of 1.3% for mean photon energy, 9.0% for photon fluence, and 9.5% for air KERMA.

	Radiological technique								
	T0	T1	T2	T3	T4	T5	T6	T7	
	Mean photon energy (keV)								
XSPMAS	62.3 ± 0.4	62.9 ± 0.4	64.1 ± 0.4	62.3 ± 0.4	62.9 ± 0.4	62.8 ± 0.4	63.4 ± 0.4	62.5 ± 0.4	
XCOMP5R	61.6		63.3	61.7	62.2	62.1	62.8	61.8	
Deviation (%)	**1.1**		**1.3**	**1.0**	**1.1**	**1.1**	**1.0**	**1.1**	**1.1** (*)
	Photon fluence ($\times 10^6$ Photon / mm^2)								
XSPMAS	$6.2 \pm 5.3\times10^3$	$2.7 \pm 2.9\times10^3$	$3.8 \pm 3.5\times10^3$	$3.9 \pm 3.5\times10^3$	$4.1 \pm 3.6\times10^3$	$4.2 \pm 3.9\times10^3$	$4.2 \pm 3.8\times10^3$	$4.2 \pm 3.8\times10^3$	
XCOMP5R	5.7	–	3.5	3.5	3.7	3.9	3.9	3.9	
Deviation (%)	**8.4**		**8.5**	**9.0**	**8.9**	**8.5**	**8.9**	**8.9**	**8.7** (*)
	Air KERMA (uGy)								
XSPMAS	225.9 ± 0.2	89.8 ± 0.1	129.8 ± 0.1	135.8 ± 0.1	141.3 ± 0.1	145.0 ± 0.12	146.9 ± 0.12	148.8 ± 0.1	
XCOMP5R	208.2		119.0	124.0	129.1	133.2	134.2	136.1	
Desviación (%)	**8.4**		**9.1**	**9.5**	**9.5**	**8.8**	**9.5**	**9.3**	**9.3** (*)

(*): Represents the average deviations for the techniques considered (from T2 to T7)

TABLE 4. *Comparison of results for the proposed radiographic techniques*

	Radiological technique								
	T0	T1	T2	T3	T4	T5	T6	T7	
	For energies of 5 – 125 keV								
AIR KERMA (uGy)	401.0 ± 0.3	160.0 ± 0.2	231.0 ± 0.2	241.0 ± 0.2	251.0 ± 0.2	281.0 ± 0.2	261.0 ± 0.2	265.0 ± 0.2	
Percentage Reduction(%)	**0.0**	**60.2**	**42.5**	**39.9**	**37.4**	**35.8**	**34.9**	**34.1**	**37.4** (*)
	For energies of 5 – 50 keV								
AIR KERMA (uGy)	159.0 ± 0.4	47.7 ± 0.2	69.1 ± 0.2	85.6 ± 0.3	87.1 ± 0.3	87.2 ± 0.3	88.4 ± 0.3	94.9 ± 0.3	
Percentage Reduction(%)	**0.00**	**70.1**	**56.7**	**46.3**	**45.4**	**45.3**	**44.5**	**40.5**	**46.5** (*)

(*): Average considering techniques T2 to T7 respectively

TABLE 5. *Percentage reduction of air KERMA, spectral comparisons*

Comparison of Air KERMA (µGy) as a Function of Energy (keV) in the Energy Range of (5 to 125) keV

Figures 4 and 5 illustrate the comparison of air KERMA as a function of energy, using technique T0 as a reference and comparing it with techniques T1 and T2, which are the most relevant radiological techniques.

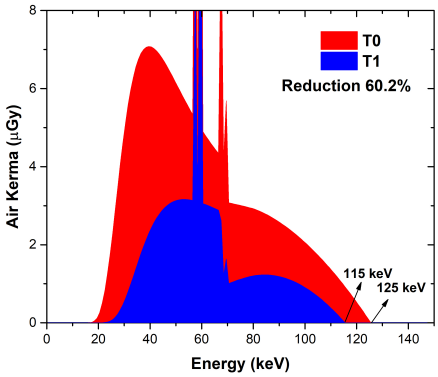

FIGURE 4. *Techniques T0 (125 kV, 0.1 mmCu, 2.0 mAs, 0.75 m) and T1 (115 kV, 0.1 mmCu + 60 µmTa, 2.0 mAs, 0.75 m)*

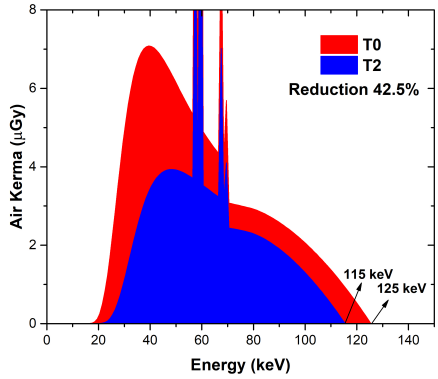

FIGURE 5. *Techniques T0 (125 kV, 0.1 mmCu, 2.0 mAs, 0.75 m) and T2 (115 kV, 0.25 mmCu, 2.0 mAs, 0.75 m)*

Comparison of Air KERMA (µGy) as a Function of Energy (keV) in the Energy Range of (5 to 125) keV

Figures 4 and 5 illustrate the comparison of air KERMA as a function of energy, using technique T0 as a reference and comparing it with techniques T1 and T2, which are the most relevant radiological techniques.

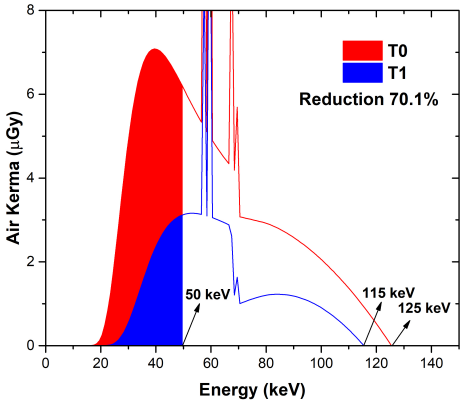

FIGURE 6. *Techniques T0 (125 kV, 0.1 mmCu, 2.0 mAs, 0.75 m) and T1 (115 kV, 0.1 mmCu+60 µmTa, 2.0 mAs, 0.75 m)*

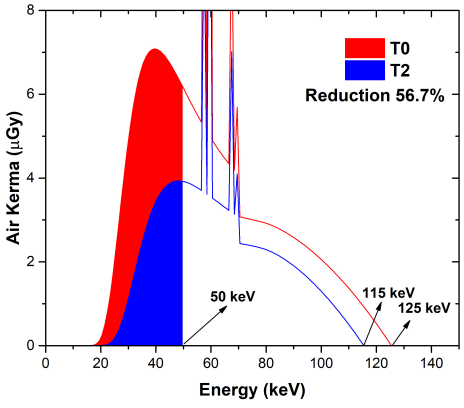

FIGURE 7. *Techniques T0 (125 kV, 0.1 mmCu, 2.0 mAs, 0.75 m) y T2 (115 kV, 0.25 mmCu, 2.0 mAs, 0.75 m)*

In Figures 4 and 5, comprehensive comparisons across the entire energy range (5 to 125 keV) are presented for each of the most relevant techniques (T1 and T2) with the reference technique (T0). The greatest reduction in x-ray fluence and consequently air kerma at the patient's entry position is achieved with the technique employing a tantalum filter, followed by

the second-highest reduction level achieved with the use of copper filters. These findings align with assessments conducted by Lopez et al. (2002), Poludniowski et al. (2007), and Poludniowski et al. (2009) [5, 15, 16].

Considering that the x-rays most contributing to cellular damage (radiological risk) are low-energy photons absorbed in the patient's skin (if we evaluate the techniques indicated in Figures 6 and 7 in the energy range of 5 to 50 keV), it is evident that it is possible to reduce the absorbed dose in the skin by up to 70,1% (for T1, using tantalum filters) and up to 56.7% (for T2, using copper filters).

The assessment of mean energies reveals maximum discrepancies of 1.8 keV, indicating the stability of this beam quality parameter. Consequently, it can be inferred that the radiographic image quality is maintained, and a positive difference suggests a potential enhancement in image quality. This assertion gains further support from the observation that the reduction in fluence within the energy range, extending from the mean energy to the maximum photon energy, experiences only a marginal decrease. This implies that fluence undergoes only a minor reduction, ensuring the preservation of image resolution.

The proposed approach was validated through the examination of medical images using the Leeds Test Objects Limited 2010 TOR CDR image quality control tool [17]. This comprehensive evaluation encompassed an assessment of both spatial resolution (High Contrast) and detection limit (Low Contrast). The results unequivocally showcased enhanced image quality with the proposed technique (T2), attributed to a reduced voltage. This reduction contributes to superior contrast, evident from the high contrast of 0.167 and low contrast of 0.011 when counting the number of discs in the radiographic image. A comparative analysis with the radiographic image obtained using the T0 reference technique for the same phantom is emphasized in Table 6.

Radiological Technique	kV	HIGH CONTRAST		LOW CONTRAST		RESOLUTION	
		Number of Discs	Contrast	Number of Discs	Contrast	Group Number	Spatial Frequency
T0	125	9	0.203	11	0.013	12	1.60
T2	115	10	0.167	12	0.011	12	1.60

TABLE 6. *Evaluation of the image quality of the reference technique, T0 (125 kV, 0.1 mmCu, 2.0 mAs, 0.75 m) and a proposed technique, T2 (115 kV, 0.25 mmCu, 2.0 mAs, 0.75 m)*

Depth Dose Distribution

Monte Carlo simulations were conducted using the X-ray spectra obtained for each radiological technique to ascertain the depth dose deposition.

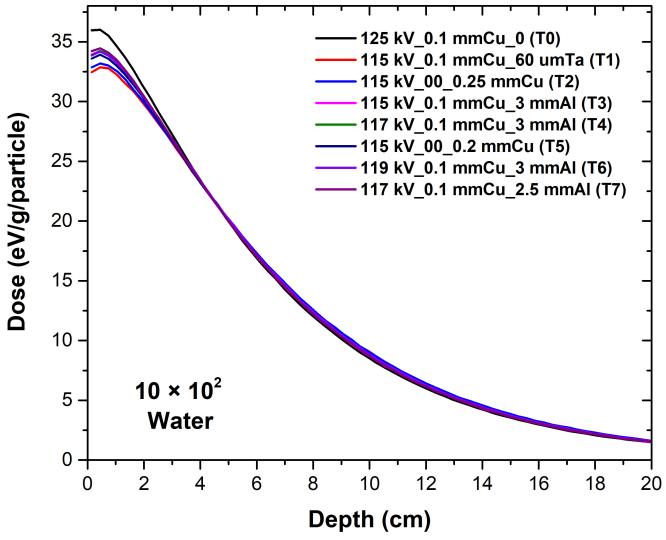

FIGURE 8. *Dose distribution function on the depth of the phantom, for the radiological techniques used*

Figure 8 illustrates the depth dose distribution per simulated particle for a 20 cm thick water phantom, encompassing all utilized radiological techniques. For a clearer depiction of dose deposition at the surface, Figure 9 has been plotted, capturing dose values from 0 to 3 cm in depth.

Figure 9 illustrates the depth dose distribution per simulated particle for all radiological techniques, showcasing that for all beam qualities, the maximum dose occurs at a depth of 0.4 cm. Radiological technique T0 deposits the highest dose at the surface, while techniques T1 and T2 deposit the least. In comparison to the reference radiological technique T0, the depth doses decrease by: 10%, 9%, 6%, 6%, 7%, 6%, and 5% for radiological techniques T1, T2, T3, T4, T5, T6, and T7, respectively.

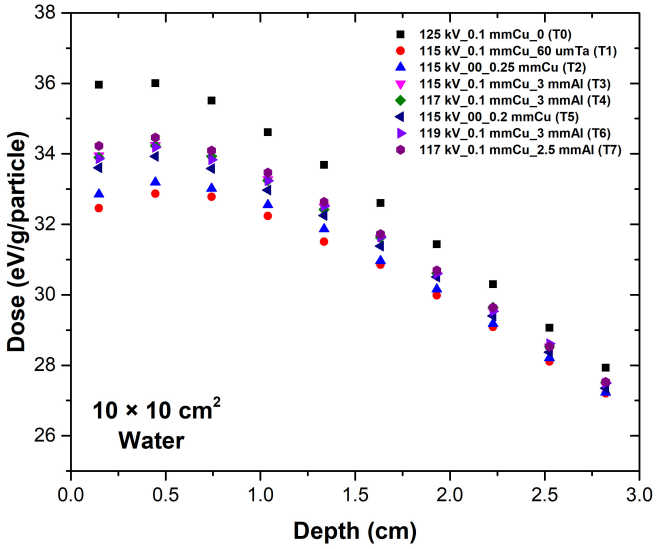

FIGURE 9. *Dose distribution function on the depth of the phantom, for the radiological techniques used.*

The reduction in absorbed dose in the skin directly contributes to preventing deterministic effects and reducing potential stochastic effects, thereby ensuring patient safety overall. Furthermore, the improvement in radiographic image quality directly enhances diagnostic precision and early detection of pathologies, while also optimizing resources.

Conclusions

The methodology developed highlights that, when employing voltages exceeding 100 kV, aluminum filters lose their efficacy in selectively attenuating the beam, especially for low-energy beams. In contrast, the use of alternative filter materials, such as copper, proves more suitable, achieving a reduction of up to 56.7% in the absorbed dose in the patient's skin.

The evaluations demonstrate a higher efficacy of the tantalum filter in reducing the absorbed dose in the patient's skin by up to 70.11%. This is attributed to tantalum's strong energy dependence of its attenuation coefficient in the X-ray energy range not useful for medical imaging, specifically between (5 to 50) keV.

Accurate knowledge of the effective energy of the X-ray beam, which can be closely approximated by the mean energy, holds paramount importance as it dictates the contrast level in the radiographic image. In this study, the calculated mean energy for the routinely used radiological technique was determined to be 62.3 keV. Consequently, the proposed techniques were carefully selected based on a criterion of +2 keV to ensure the preservation of the same level of image contrast, thus reproducing comparable or superior image quality.

Thus, it is concluded that, with the developed methodology based on the assessment of X-ray spectra, it is possible to reduce the absorbed dose received by patients in diagnostic X-ray examinations by up to 56.7% (with the use of copper filters) and up to 70.11% (with the use of tantalum filters). Consequently, a reduction in radiological risk is ensured at these percentages, guaranteeing the quality and safety of radiological procedures involving the use of X-rays.

Even with the findings presented in this study, the developed method offers a complementary approach for conducting quality control on diagnostic X-ray equipment. It demonstrates advantages such as a straightforward calculation process and time savings in characterizing the X-ray spectrum used in clinical settings.

References

[1] ICRP, *Managing Patient Dose in Digital Radiology*, Vol. 34 (ICRP Publication 93, 2004).

[2] B. Müller, J. Singer, and et al., Rofo **194**, 400 (2022).

[3] OTAN, Lesión dérmica radioinducida al paciente con siglas AAGA. resolución directoral no. 2240-22-ipen/otan (2022).

[4] IPEN, Lesión dérmica radioinducida al paciente con siglas AAGA. resolución de presidencia no. d000188-2022-ipen-pres (2022).

[5] G. Poludniowski, Med. Phys. **34**, 2175 (2007).

[6] K. Peglow, M. Yuamoto, and et al., *Use of additional filters for optimization of the chest X-ray examination protocol using CDRAD Phantom simulator* (Congress: EuroSafe Imaging 2021, Poster Number: ESI-11867).

[7] F. Salvat, J. Fernández, and J. Sempau, *Quantum phase transitions and structural evolution in nuclei* (PENELOPE-2018: Workshop proceedings, 2019).

[8] M. Córte Brochi, *Métodos de Simulação Computacional para Redução de Dose em Radiodiagnóstico. Departamento de física, Universidad de São Paulo*, Master's thesis (1990).

[9] R. Nowotny and A. Höfer, Rofo **142**, 685 (1985).

[10] R. Birch and M. Marshall, Phys. Med. Biol. **24**, 505 (1979).

[11] T. Benavente, J. Márquez, and J. S. Cruz, Revista de investigación de Física, UNMSM **2**, 52 (1999).

[12] N. Dyson, Phys. Med. Biol. **20**, 1 (1975).

[13] A. Brosed, *Fundamentos de Física Médica*, Vol. 1 (SEFM, 2012).

[14] M. Berger, J. Hubbell, and et al., XCOM: Photon Cross Section Database, Version 1.3, NIST (2007).

[15] A. López, F. Salvador, and et al., Radioprotección **32**, 5 (2002).

[16] G. Poludniowski, Med. Phys. **34**, 2175 (2007).

[17] Leeds Test Objects Limited, *Leeds Test Objects, TOR CDR (Manual)* (2005).